MMSE CHANNEL PREDICTION FOR SYMBOL-BY-SYMBOL ADAPTIVE OFDM SYSTEMS

M. Münster and L. Hanzo[1]

Dept. of Electronics and Computer Science,
University of Southampton, SO17 1BJ, UK.
Tel: +44-1703-593 125, Fax: +44-1703-594 508
Email:lh@ecs.soton.ac.uk
http://www-mobile.ecs.soton.ac.uk

ABSTRACT

Subband Adaptive Orthogonal Frequency Division Multiplexing (OFDM) constitutes an effective method of compensating for the frequency selective fading incurred by mobile receivers. The channel transfer function estimation error increases as a function of the Doppler frequency and of the subband modem mode signalling delay. This leads to a degradation of the system performance. In this contribution a *2D-MMSE channel-predictor* is investigated as a means of compensating for these effects, which incorporates the scheme proposed in [1] into adaptive OFDM.

1. OVERVIEW

Subband adaptive OFDM (AOFDM) has been shown to be an effective method of improving the system performance in mobile environments, where the subbands least affected by frequency-selective fading are assigned more bits per subcarrier, than the severely faded subbands [2–4]. The modulation mode assignment to be employed by the remote transmitter A in the next timeslot is determined by the local receiver B upon invoking an estimate of the short-term channel quality experienced by the most recently received OFDM symbol. Due to the channel's variation with time, there is a mismatch between the channel quality estimated by receiver B and that actually experienced by the following OFDM symbol transmitted by transmitter A. This reduces the achievable performance gain of AOFDM compared to employing a single fixed modulation mode. Hence the application of AOFDM is confined to channel environments exhibiting relatively low Doppler frequencies if no channel prediction is used. Hence, in order to support AOFDM in a broader range of mobility conditions, signal prediction techniques - which are well-known from the field of speech-coding for example - can be employed for obtaining a more accurate estimate of the channel quality in the next transmission timeslot on the basis of that in previous slots. A channel predictor assisted OFDM pre-equalization scheme was discussed in [5], while prediction assisted decision-directed channel estimation has been proposed in [6]. In our contribution we will study the performance of an AOFDM transceiver, which employs decision-directed channel estimation and modulation mode adaptation. In the next section we will commence our discussions with an outline of the adaptive transceiver structure, while in Section 3 we detail two channel estimator designs. Finally, in Section 4 the system's performance is evaluated under a variety of channel conditions.

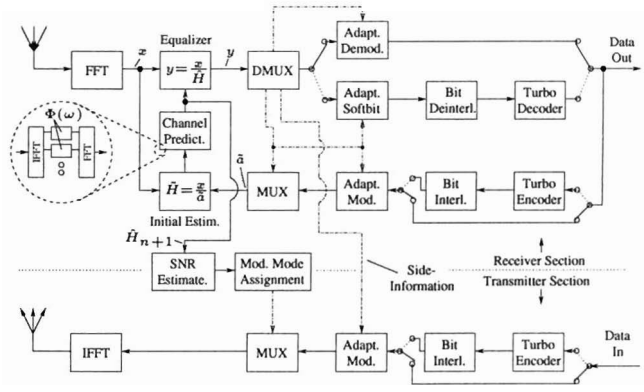

Figure 1: Schematic of the subband adaptive transceiver employing decision-directed MMSE *channel prediction.*

2. DESCRIPTION OF THE ADAPTIVE TRANSCEIVER

The schematic of the adaptive time division duplex (TDD) transceiver employed in our simulations is shown in Figure 1. The signal received from the remote transmitter A in the n-th downlink timeslot is forwarded to a Fast Fourier Transform (FFT) block, followed by the frequency-domain equalization of the complex symbols associated with each of the K subcarriers. Equalization ensues using the channel transfer function estimate $\hat{H}[n,k]$, $k \in \{1,\ldots,K\}$ pre-

5^{th} INTERNATIONAL OFDM WORKSHOP, SEPTEMBER 12^{th} AND 13^{th}, HAMBURG, GERMANY

The financial support of the European Union under the auspices of the Pan-European TRUST project and that of the EPSRC, Swindon UK is gratefully acknowledged

dicted during the $(n-1)$-th downlink timeslot on the basis of the OFDM symbols transmitted in the previous P downlink timeslots, where each timeslot hosts one OFDM symbol. The subband modulation mode assignment requested by receiver B from transmitter A for the current downlink OFDM symbol as well as the modulation mode assignment to be employed by transmitter B for the OFDM symbol transmitted on the next uplink timeslot is explicitely embedded into the data stream as side-information. As seen in Figure 1, the primary data and the modem mode signalling streams are separated from each other in the demultiplexer (DMUX) stage of Figure 1, followed by adaptive OFDM demodulation of the primary user data. Additionally, turbo coding can be employed in the system, which requires adaptive soft-bit generation at the receiver instead of direct hard-decision based adaptive demodulation, followed by channel-deinterleaving and turbo decoding. The demodulated and turbo decoded data stream is conveyed to the adaptive receiver's output. Furthermore, the sliced bits are invoked to regenerate the transmitted OFDM symbol to be used as a reference signal, which allows updating the channel estimate generated by the receiver. Hence the output bit stream has to be optionally re-encoded and re-modulated. An initial estimate $\tilde{H}[n,k]$ of the actual channel transfer function $H[n,k]$ in the k-th subcarrier of the n-th OFDM symbol is obtained upon dividing the complex received OFDM symbol $x[n,k]$ by the subcarrier's sliced symbol $\tilde{a}[n,k]$ [1], yielding:

$$\begin{aligned} \tilde{H}[n,k] &= \frac{x[n,k]}{\tilde{a}[n,k]}, \; k \in \{0,\ldots,K-1\} \\ &= H[n,k] \cdot \frac{a[n,k]}{\tilde{a}[n,k]} + \frac{w[n,k]}{\tilde{a}[n,k]}, \end{aligned} \quad (1)$$

where $H[n,k]$ denotes the Rayleigh-distributed complex channel transfer function with variance σ_h^2, which is of unity. Furthermore, $a[n,k]$ represents the complex OFDM symbol transmitted, which exhibits zero mean and a variance of σ_s^2, and finally $w[n,k]$ is the Additive White Gaussian Noise (AWGN) contribution with a mean value of zero and variance σ_n^2. The total noise variance σ_n^2 is constituted by the sum of the AWGN process' variance σ_{AWGN}^2 plus the variance of the Gaussian noise-like inter-subcarrier interference contribution σ_{ICI}^2. The latter component can be neglected in fading channels exhibiting a low maximum Doppler frequency $f_{d,max}$. However, under high-mobility channel conditions - which we envisage for our system - an estimate of σ_{ICI}^2 has to be provided. Upon assuming error-free symbol decisions, where $\tilde{a}[n,k] = a[n,k]$, the initial channel transfer function estimate of Equation 1 is simplified to:

$$\tilde{H}[n,k] = H[n,k] + \frac{w[n,k]}{a[n,k]}, \quad (2)$$

which has a mean-square estimation error of $\beta[n,k]\sigma_n^2/\sigma_s^2$. The factor $\beta[n,k]$ depends on the modulation mode employed in the k-th subcarrier. For an M-PSK mode for example, $\beta[n,k] = 1$, while for the 16-QAM modulation mode $\beta[n,k] = 17/9$ [7]. A minimum mean-square error (MMSE) channel estimator was proposed in [1], in order to infer more accurate channel transfer function estimates $\hat{H}[n,k]$ from the initial channel estimates $\tilde{H}[n,k]$. This is achieved by additionally capitalizing on the previous initial estimates $\tilde{H}[n-\nu,k]$, $\nu \in \{1,\ldots,P-1\}$, $k \in \{0,\ldots,K-1\}$ of the $(P-1)$ past OFDM symbols, where $P-1$ denotes the order of the associated interpolation filter. This estimator exhibits the structure seen in Figure 1, within the circle drawn in dashed lines. Explicitely, from the frame of initial channel transfer function estimates $\tilde{H}[n,k]$ of the most recently received OFDM symbol, initially a short-term estimate of the time-variant channel impulse response (CIR) is obtained upon invoking the Inverse Fast Fourier Transform (IFFT). Only the first K_0 time-domain CIR samples are retained, while the higher-delay IFFT output samples constituted by noise are set to zero in order to mitigate the effects of noise by a factor of K_0/K. Furthermore, Wiener filtering is performed [1], which will be contrasted to channel prediction [6] in Section 3, in order to further reduce the impact of the channel noise and also to render the CIR estimator more robust against the adverse effects of erroneous symbol decisions. Lastly, the FFT is applied to the CIR estimate, in order to obtain the refined estimates $\hat{H}[n,k]$ of the frequency domain channel transfer function of the *current* OFDM symbol. In [1] this estimate was employed for the frequency domain equalization of the *next* received OFDM symbol, neglecting the channel's Doppler-dependent variation. Furthermore, it was demonstrated in [1] that the CIR estimator is robust against a mismatch between the maximum CIR delay spread of $\tau = (K_0 - 1)T_s$ imposed during the above noise-reduction process - where T_s is the sampling period of the OFDM system - and the maximum delay spread τ_{max} actually experienced. The CIR estimator was also found insensitive [1] against a mismatch between the assumed maximum Doppler frequency f_d in comparison to $f_{d,max}$ actually experienced, for values of $\tau \geq \tau_{max}$ and $f_d \geq f_{d,max}$. In channel evironments exhibiting a relatively high degree of mobility the mismatch between the channel transfer function $\hat{H}[n,k]$ estimated for the current OFDM symbol, but also employed for equalization of the next received OFDM symbol, may be excessive. Hence, in order to avoid this mismatch, the motivation of [6] was to employ a prediction filter instead of the interpolation filter of [1]. This scheme was also incorporated in the adaptive transceiver structure portrayed in Figure 1. In the proposed arrangement the advantage of employing a prediction filter is two-fold. Firstly, more accurate CIR estimates are provided in the context of decision-directed channel estimation. Secondly, the channel quality expressed in terms of the signal-to-noise ratio (SNR) and potentially experienced by an OFDM symbol in the next downlink timeslot can be estimated more reliably. This potentially enhances the performance of our AOFDM scheme. The design of the prediction filter will be further elaborated on in Section 3. The AOFDM mode adaptation performed by the modem is based on the choice between a set of four modulation modes, namely 4, 2, 1 and 0 bit/subcarrier, where the latter mode corresponds to 'no transmission'. The modulation mode could be in theory assigned on a subcarrier-by-subcarrier basis, but the signalling overhead of such a system would be prohibitive, without significant performance advantages [2]. Hence, we have grouped adjacent subcarri-

ers into 'subbands' and assigned the same modulation mode to all subcarriers in a subband [2, 3]. Note that the frequency domain channel transfer function is typically not constant across the subcarriers of a subband, hence the modem mode adaptation will be sub-optimal for some of the subcarriers. The modem mode adaptation is achieved on the basis of the SNR estimated in each of the K subcarriers for the OFDM symbol hosted by the $(n+1)$-th downlink timeslot, which is formulated as:

$$SNR[n+1,k] = \hat{H}^2[n+1,k]\frac{\sigma_s^2}{\sigma_n^2}. \quad (3)$$

The iterative AOFDM mode assignment commences by calculating in the first step for each subband and for all four modulation modes the expected overall subband bit error rate (BER) by means of averaging the estimated individual subcarrier BERs [2]. Throughout the second step of the algorithm - commencing with the lowest throughput but most robust modulation mode in all subbands - in each iteration the number of bits/subcarrier of that particular subband is increased, which provides the best compromise in terms of increasing the number of expected bit errors and the number of additional data bits accommodated. This process continues, until the target number of bits to be transmitted by the OFDM symbol is reached. This algorithm originates from the philosophy of the Hughes-Harthogs algorithm [8]. As a result of intensive research in the area recently several computationally efficient versions of the algorithm have emerged [2]. Again, the computed AOFDM mode assignment is explicitely signalled to the remote transmitter A on the next uplink OFDM symbol transmitted by transmitter B for employment in the forthcoming downlink timeslot. In the next section the design of the CIR predictor will be outlined.

3. THE MMSE-PREDICTOR

In this section we briefly highlight the structure of the MMSE predictor [9,10]. An estimate $\hat{h}[n+1,\acute{k}]$ of the $\acute{k}$-th CIR tap, where $\acute{k} < K_0$, is given by:

$$\hat{h}[n+1,\acute{k}] = \sum_{\nu=0}^{P-1} c[\nu,\acute{k}] \cdot \tilde{h}[n-\nu,\acute{k}], \quad (4)$$

for the $(n+1)$-th timeslot. In Equation 4 the variable $c[\nu,\acute{k}]$ denotes the ν-th coefficient of the P-tap predictor and $\tilde{h}[n-\nu,\acute{k}]$ represents the initial estimate of the $\acute{k}$-th CIR tap in the $(n-\nu)$-th timeslot, which is related to the initial estimates $\tilde{H}[n-\nu,k]$ of the channel transfer function values by the Discrete Fourier Transform (DFT). Upon invoking Equation 4, the squared error between the true CIR value $h[n+1,\acute{k}]$ and the estimated CIR value $\hat{h}[n+1,\acute{k}]$ can be expressed as:

$$\begin{aligned} |e|^2 &= \left|h[n+1,\acute{k}] - \hat{h}[n+1,\acute{k}]\right|^2 \\ &= \left|h[n+1,\acute{k}] - \sum_{\nu=0}^{P-1} c[\nu,\acute{k}] \cdot \tilde{h}[n-\nu,\acute{k}]\right|^2. \end{aligned} \quad (5)$$

For notational simplicity and since the sets of filter coefficients employed for predicting different CIR taps are identical - as a consequence of the channel correlation function's separability - the CIR tap index $\acute{k}$ will be omitted from now on. By differentiating Equation 5 with respect to each of the CIR predictor coefficients $c[\kappa]$, $\kappa \in \{0,\ldots,P-1\}$, a set of P equations can be obtained, which are known in the literature as the Wiener-Hopf equations [10] given by:

$$\begin{aligned} \sum_{\nu=0}^{P-1} c^*[\nu] \cdot E\{\tilde{h}[n-\kappa] \cdot \tilde{h}^*[n-\nu]\} &= \\ E\{\tilde{h}[n-\kappa] \cdot h^*[n+1]\}, \end{aligned} \quad (6)$$

where again $\kappa \in \{0,\ldots,P-1\}$ and $E\{\}$ denotes the expected value. By introducing vector notation, a more convenient representation of Equation 6 can be found:

$$\mathbf{R_t} \cdot \mathbf{c} = \mathbf{r_t}, \quad (7)$$

where the $(P \times P)$-auto-covariance matrix $\mathbf{R_t}$ of the initial CIR tap estimates used for predicting the $\acute{k}$-th CIR tap is given by:

$$\mathbf{R_t} = E\{\tilde{\mathbf{h}} \cdot \tilde{\mathbf{h}}^H\} = E\{\mathbf{h} \cdot \mathbf{h}^H\} + \frac{K_0}{K}\frac{\sigma_n^2}{\sigma_s^2}\mathbf{I}. \quad (8)$$

Observe in Equation 8 the increase of the acutally perceived $SNR = \sigma_s^2/\sigma_n^2$ by a factor of K/K_0, as a result of setting the CIR taps above the index (K_0-1) to zero, as outlined in Section 2. Furthermore, we have neglected the effects of the modulation mode-dependent SNR variations alluded to earlier in Section 2. The $(P \times 1)$-cross-covariance vector $\mathbf{r_t}$ seen in Equation 7 is defined by:

$$\mathbf{r_t} = E\{\tilde{\mathbf{h}} \cdot h^*[n+1]\} = E\{\mathbf{h} \cdot h^*[n+1]\}. \quad (9)$$

Furthermore, $\tilde{\mathbf{h}}$ is the $(P \times 1)$-sample vector containing the $\acute{k}$-th tap of the P initial CIR estimates:

$$\tilde{\mathbf{h}} = \left(\tilde{h}[n], \tilde{h}[n-1], \ldots, \tilde{h}[n-(P-1)]\right)^T, \quad (10)$$

and $\mathbf{c}$ is the $(P \times 1)$-vector of CIR predictor coefficients:

$$\mathbf{c} = (c^*[0], c^*[1], \ldots, c^*[n-(P-1)])^T. \quad (11)$$

A conceptually straightforward solution of Equation 7 for $\mathbf{c}$ is given by the direct inversion of the auto-covariance matrix $\mathbf{R_t}$:

$$\mathbf{c} = \mathbf{R_t}^{-1} \cdot \mathbf{r_t}. \quad (12)$$

However, computationally more efficient approaches such as the Levinson-Durbin algorithm [10] are available, which take into account the Töplitz structure of the auto-covariance matrix that is stated as $\mathbf{R_t}^T = \mathbf{R_t}^*$. The MSE of the estimator is given by rearranging Equation 5 and calculating the expected value of $|e|^2$, yielding [10]:

$$MSE = \sigma_h^2 - \mathbf{c}^H \cdot \mathbf{r_t} - \mathbf{c}^T \cdot \mathbf{r_t}^* + \mathbf{c}^H \cdot \mathbf{R_t} \cdot \mathbf{c}, \quad (13)$$

where the channel variance σ_h^2 was defined in Section 2 to be of unity. The difference between the predictior [6] employed in our system portrayed in Figure 1 and the interpolation filter proposed in [1] is in the definition of the cross-covariance vector of Equation 12. Specifically, the *predictor* employs an estimate of the cross-covariance between the $\acute{k}$-th CIR taps $\tilde{h}[n-\nu]$, $\nu \in \{0,\ldots,P-1\}$ of the previous $P-1$ plus

the current CIRs and the actual $\acute{k}$-th CIR tap $h[n+1]$ expected during the $(\mathbf{n+1})$-**th** OFDM symbol. By contrast, the *interpolator* capitalizes on the cross-covariance between the $\tilde{k}$-th CIR taps of the previous $P-1$ plus the current CIRs and the actual $\acute{k}$-th CIR tap $h[n]$ expected during the **n-th** OFDM symbol, which belongs to the current timeslot. One of the main aspects highlighted in the context of Li's treatise on decision-directed channel estimation in [1] was that in order to render the time-domain Wiener interpolation filter robust against a mismatch between the Doppler frequency f_d assumed in the filter design and the maximum Doppler frequency $f_{d,max}$ actually exhibited by the channel, the Doppler power spectral density had to be ideally bandlimited to f_d, where $f_d \geq f_{d,max}$. Hence, the covariance values $E\{h[n-\gamma] \cdot h^*[n-\delta]\}$ were expressed as:

$$E\{h[n-\gamma] \cdot h^*[n-\delta]\} = \frac{sin((\gamma-\delta)2\pi f_d T_{td})}{(\gamma-\delta)2\pi f_d T_{td}}, \qquad (14)$$

where f_d denotes the Doppler frequency and T_{td} is the time-domain delay between two consecutive OFDM symbols. Hence T_{td} also corresponds to the time-domain separation of the $\tilde{k}$-th taps of two consecutive CIR estimates. Hence, in the TDD system described in Section 2, T_{td} is the time-domain delay between two consecutive uplink- or downlink timeslots, which is twice the OFDM symbol duration, if alternate uplink and downlink timeslots are used. In the next section we will embark on the performance assessment of the proposed system.

4. SIMULATION RESULTS

In this section the performance of the decision-directed channel estimation assisted subband adaptive OFDM transceiver will be assessed in the context of the indoor Wireless Asynchronous Transfer Mode (WATM) channel environment characterized by the short (S)CIR of [2], which we hence refer to in our figures as the SWATM channel. In Figure 2 we have portrayed the performance of the AOFDM modem for two different normalized Doppler frequencies $f_{d,max}T_f$, where T_f denotes the OFDM symbol duration. Explicitely, this implies that the Doppler frequency was normalised to the OFDM symbol duration, rather than to the time-domain sampling interval duration, typically used in single-carrier modems. For these simulations we assumed perfect channel transfer function knowledge, zero-delay signalling of the AOFDM modulation mode assignment and 'frame-invariant' fading, where the CIR taps were kept constant for the duration of an OFDM symbol, in order to avoid inter-subcarrier interference. We observe - particularly for SNRs in excess of 20dB, where potentially all of the available AOFDM modulation modes were invoked - that the BER performance is significantly degraded under high-Doppler channel conditions. Similar investigations were conducted in Figure 3, where the assumption of zero-delay signalling of the AOFDM modulation mode assignment was removed in favour of the more realistic TDD scenario. Explicitely, the modulation mode assignment requested by receiver B for the next downlink timeslot was signalled by transmitter B to receiver A in the uplink slot. We observed a further degradation as a result of the increased CIR estimation delay T_{td}, which was $2T_f$ for the TDD scenario. Let us now focus our attention on the channel transfer function prediction as a measure of combating these effects.

In Figure 4 we have plotted the mean-square channel estimation error (MSE) exhibited by the CIR predictor in the indoor SWATM channel environment [2] under various conditions of mobility and for prediction filter lengths of 1, 2 or 4 OFDM symbols. Since in these simulations error-free OFDM symbols were assumed for reference generation, the portrayed MSE is independent of the modulation modes actually used. We observed that the MSE performance significantly improved upon increasing the filter length. The MSE floor apparent for higher SNRs as a result of the Doppler-dependent channel variation was virtually removed for the $f_{d,max}T_f$ values considered, by employing a 4-tap channel predictor. Our investigations revealed that higher predictor lengths resulted mainly in a reduction of the noise's influence, which was indicated by a parallel shift of the MSE curves towards lower average channel SNR values. Having demonstrated that the predictor is capable of efficiently compensating for the channel's Doppler-dependent transfer function variations, we will now embark on the assessment of its performance in the context of the adaptive transceiver described in Section 2.

In our forthcoming simulations the idealistic assumptions of 'frame-invariant' fading and zero-delay signalling were removed, again, in favour of the 'frame-variant' fading TDD scenario. The uncoded BER performance is illustrated in Figures 5 and 6. In Figure 5 we characterised the low-mobility scenario of $f_{d,max}T_f = 0.01$ while in Figure 6 the high-mobility scenario $f_{d,max}T_f = 0.05$. As a reference, we have plotted in both figures the performance exhibited by the fixed BPSK and QPSK modulation modes, employing a 4-tap predictor. Upon invoking AOFDM modulation we observed - particularly for the 4-tap predictor - a tremendeous performance gain over the fixed modulation modes. The improvement was more dramatic for the high-mobility environment associated with Figure 6, where a BER floor was observed at high SNRs as a result of the fading-induced inter-subcarrier interference. In this scenario, low-BER transmission was infeasible without CIR prediction. For relatively low SNRs the BER performance was more limited as a result of erroneous symbol decisions in the initial CIR estimation stage of the decision-directed channel estimator. This effect was a consequence of employing only one known OFDM training symbol for the initial channel transfer function acquisition, but an improvement could be achieved by periodically inserting known training OFDM symbols. In Figure 7 we have also plotted the BER performance of the turbo-coded AOFDM transceiver, where the channel estimation also benefitted from the turbo-decoding, since the re-encoded AOFDM symbols used as a channel estimation reference were less impaired by erroneous symbol decisions. The figures reflect the turbo decoder's typical behaviour, where the BER rapidly decreases, once the SNR is above a certain threshold.

In conclusion, we have demonstrated that by invoking MMSE CIR prediction efficient decision-directed channel estimation can be successfully employed in conjunction with

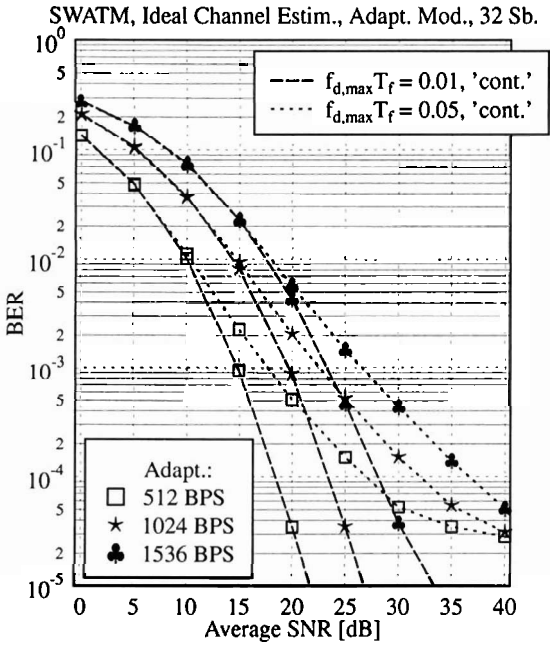

Figure 2: **Influence of the normalized Doppler frequency** on the BER performance of the 32-subband 512-subcarrier AOFDM modem in the 'frame-invariant' fading indoor SWATM environment of [2] assuming zero-delay modulation mode signalling and perfect channel transfer function knowledge. In the legend, 'cont.' indicates continous zero-delay modem mode signalling. The number of Bits per AOFDM Symbol (BPS) was 512, 1024 and 1536.

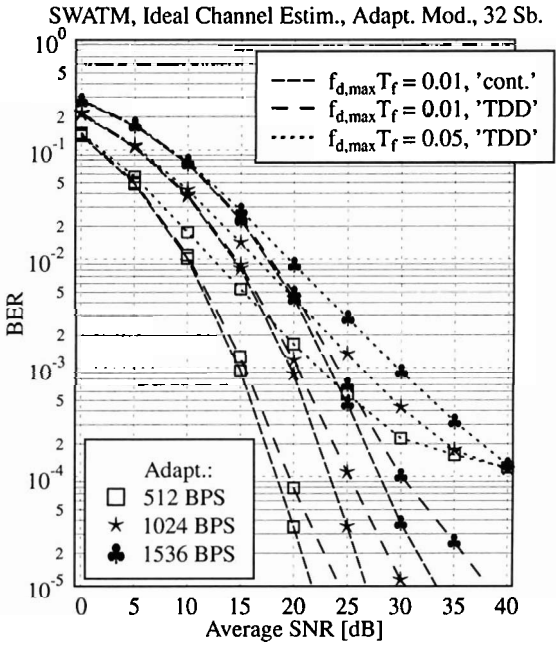

Figure 3: **Influence of the normalized Doppler frequency and the modulation mode signalling delay** on the BER performance of the 32-subband 512-subcarrier AOFDM modem in the 'frame-invariant' fading indoor SWATM environment [2] assuming perfect channel transfer function knowledge. The AOFDM mode signalling delay was 0 ('cont.') or 1 AOFDM symbol duration (TDD) and 512, 1024 and 1536 bits per OFDM symbol were transmitted.

AOFDM even under high-mobility channel conditions.

5. REFERENCES

[1] Y. Li, L. J. Cimini, and N. R. Sollenberger, "Robust Channel Estimation for OFDM Systems with Rapid Dispersive Fading Channels," *IEEE Trans. on. Comms.*, vol. 46, pp. 902–915, Apr 1998.

[2] L. Hanzo, W. Webb, and T. Keller, *Single- and Multi-carrier Quadrature Amplitude Modulation.* IEEE Press- John Wiley, April 2000.

[3] T. Keller and L. Hanzo, "Adaptive Orthogonal Frequency Division Multiplexing Schemes," in *Proc. ACTS'98 Summit*, (Rhodos, Greece), pp. 794–799, June 1998.

[4] H. Rohling and R. Gruenheid, "Adaptive Coding and Modulation in an OFDM-TDMA Communication System," in *Vehicular Technology Conference*, vol. 2, (Ottawa, Canada), pp. 773–776, IEEE, May 18-21 1998.

[5] F. Tufvesson, M. Faulkner, and T. Maseng, "Pre-Compensation for Rayleigh Fading Channels in Time Division Duplex OFDM Systems," in *Proc. of 6th International Workshop on Intelligent Signal Processing and Communications Systems*, (Melbourne, Australia), pp. 57–33, IEEE, November 5-6 1998.

[6] E. Al-Susa and R. F. Ormondroyd, "A Predictor-Based Decision Feedback Channel Estimation Method for COFDM with High Resilience to Rapid Time-Variations," in *Proc. of Vehicular Technology Conference*, vol. 1, (Amsterdam, Netherlands), pp. 273–278, IEEE, September 19-22 1999.

[7] O. Edfors, M. Sandell, J.-J. v. d. Beek, S. K. Wilson, and P. O. Börjesson, "OFDM Channel Estimation by Singular Value Decomposition," *IEEE Trans. on. Comms.*, vol. 46, pp. 931–939, Apr 1998.

[8] D. Hughes-Hartogs, "Ensemble modem structure for imperfect transmission media," *U.S. Patents Nos. 4,679,222 (July 1987), 4,731,816 (March 1988) and 4,833,796 (May 1989).*

[9] A. Duel-Hallen, S. Hu, and H. Hallen, "Long Range Prediction of Fading Signals," *IEEE Signal Processing Magazine*, vol. 17, pp. 62–75, May 2000.

[10] S. Haykin, *Adaptive Filter Theory.* Prentice Hall, Inc., 1996.

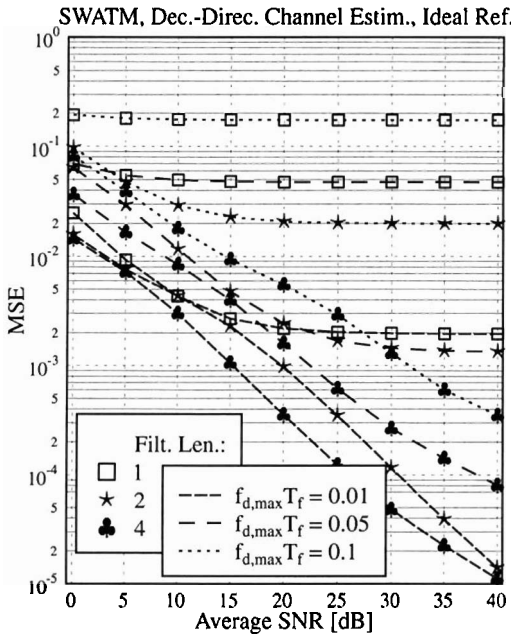

Figure 4: **Influence of the CIR predictor length and the normalized Doppler frequency** on the MSE performance of the decision-directed channel predictor in the 'frame-invariant' fading indoor SWATM environment [2] using error free OFDM symbols for reference generation.

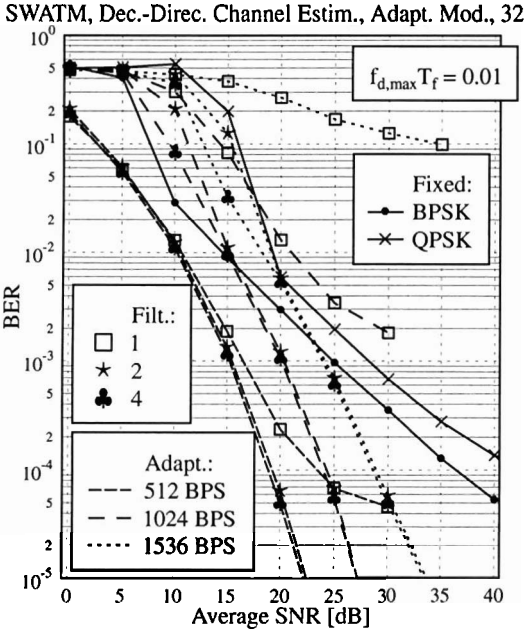

Figure 5: **Influence of the predictor length and the target bitrate** (Bits Per OFDM Symbol) on the BER performance of the decision-directed channel prediction assisted 32-subband 512-subcarrier AOFDM modem in the 'frame-variant' fading indoor SWATM environment [2] exhibiting a normalized Doppler frequency of $f_{d,max}T_f = 0.01$.

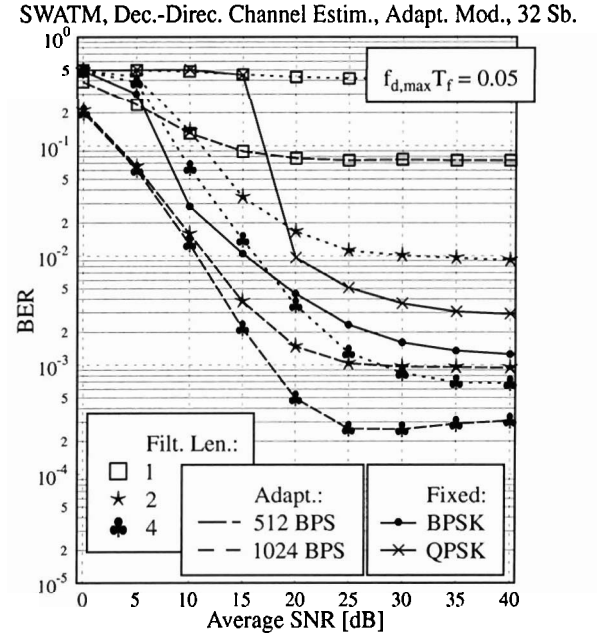

Figure 6: **Influence of the predictor length and the target bitrate** on the BER performance of the decision-directed channel prediction assisted 32-subband 512-subcarrier AOFDM modem in the 'frame-variant' fading indoor SWATM environment [2] exhibiting a normalized Doppler frequency of $f_{d,max}T_s = 0.05$.

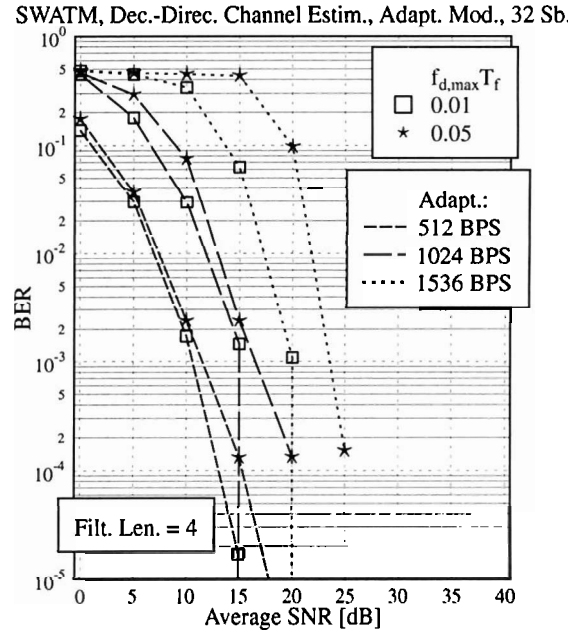

Figure 7: **Influence of the normalized Doppler frequency and the target bitrate** on the BER performance of the decision-directed 4-tap channel prediction assisted 32-subband 512-subcarrier **turbo-coded** AOFDM modem in the 'frame-variant' fading indoor SWATM [2] environment.